

Weyl semimetal emitter enabling TE-polarized wide-angle nonreciprocal thermal radiation

Jingcheng Yu(于晶城), Jimin Fang(方记民), Jiaqi Zou(邹佳琦), Tingyu Liu(刘庭瑜), Manzhuo Wang(王曼卓), Xiaoqiang Sun(孙小强), Yuanda Wu(吴远大), Daming Zhang(张大明)

Citation: Chin. Phys. B. 35, 094206 (2026). DOI: 10.1088/1674-1056/ae1c32 |
CSTR: 32038.14.CPB.ae1c32
http://cpb.iphy.ac.cn; http://iopscience.iop.org/cpb

What follows is a list of articles you may be interested in

Intrinsic polarization conversion and avoided-mode crossing in X-cut lithium niobate microrings

Zelin Tan(谭泽林), Jianfa Zhang(张检发), Zhihong Zhu(朱志宏), Wei Chen(陈伟), Zhengzheng Shao(邵铮铮), Ken Liu(刘肯), Shiqiao Qin(秦石乔)
Chin. Phys. B. 33, 064205 (2024). DOI: 10.1088/1674-1056/ad47b2

Compact TE-pass polarizer based on lithium-niobate-on-insulator assisted by indium tin oxide and silicon nitride

Jia-Min Liu(刘家敏), De-Long Zhang(张德龙)
Chin. Phys. B. 32, 064208 (2023). DOI: 10.1088/1674-1056/ac960b

High efficiency of Brillouin scattering behavior in single-mode Ge–As–Se–Te fibers at 2 μm

Yue Fu(付悦), Shi-Xun Dai(戴世勋), Lu-Lu Xu(徐路路), Yao-Jun Fang(方耀俊), Ying-Ying Wang(王莹莹), Kai Jiao(焦凯), Xun-Si Wang(王训四)
Chin. Phys. B. 32, 054206 (2023). DOI: 10.1088/1674-1056/ac9a3a

Bound states in the continuum in metal—dielectric photonic crystal with a birefringent defect

Hongzhen Tang(唐宏珍), Peng Hu(胡鹏), Da-Jian Cui(崔大健), Hong Xiang(向红), Dezhuan Han(韩德专)
Chin. Phys. B. 31, 104209 (2022). DOI: 10.1088/1674-1056/ac6db6

High-performance and fabrication friendly polarization demultiplexer

Huan Guan(关欢), Yang Liu(刘阳), Zhiyong Li(李智勇)
Chin. Phys. B. 31, 034203 (2022). DOI: 10.1088/1674-1056/ac21bc

Weyl semimetal emitter enabling TE-polarized wide-angle nonreciprocal thermal radiation

Jingcheng Yu(于晶城)[1], Jimin Fang(方记民)[1], Jiaqi Zou(邹佳琦)[1], Tingyu Liu(刘庭瑜)[1], Manzhuo Wang(王曼卓)[1], Xiaoqiang Sun(孙小强)[1,†], Yuanda Wu(吴远大)[2,3], and Daming Zhang(张大明)[1]

[1] *State Key Laboratory of Integrated Optoelectronics, College of Electronic Science and Engineering, Jilin University, Changchun* 130012, *China*

[2] *College of Materials Science and Opto-Electronic Technology, University of Chinese Academy of Sciences, Beijing* 100049, *China*

[3] *Key Laboratory of Optoelectronic Materials and Devices, Institute of Semiconductors, Chinese Academy of Sciences, Beijing* 100083, *China*

(Received 19 September 2025; revised manuscript received 3 November 2025; accepted manuscript online 6 November 2025)

Wide-angle nonreciprocal thermal radiation that deviates from Kirchhoff's law over a broad angular range is relevant for energy harvesting and thermal management. Although wide-angle nonreciprocity for TM-polarized waves has been demonstrated, a comparable effect for TE polarization remains challenging due to reciprocity constraints. A TE-polarized nonreciprocal thermal emitter composed of a Ge grating, Weyl semimetal, and a planar Ag layer is proposed. High emission and low absorption for TE polarization across the azimuthal range from 20° to 80° with nonreciprocity exceeding 0.7 can be obtained. The results indicate that the emitter maintains consistent emission despite dimensional variations, demonstrating favorable fabrication tolerance. The TE-polarized wide-angle nonreciprocity remains stable against minor fluctuations in temperature and axial vector. This proposed approach extends nonreciprocal thermal radiation beyond TM polarization while providing flexibility in wide-angle emission control. It has potential in nonreciprocal radiative cooling, thermophotovoltaics, and infrared technologies.

Keywords: TE-polarized, nonreciprocal thermal radiation, wide-angle emission, Weyl semimetals

PACS: 42.25.Ja, 44.40.+a, 78.20.Ls, 81.05.Xj

DOI: 10.1088/1674-1056/ae1c32 **CSTR:** 32038.14.CPB.ae1c32

1. Introduction

Nonreciprocal thermal radiation (NTR), an emerging technology distinct from conventional thermal emitters, offers significant potential for energy harvesting and conversion. According to Kirchhoff's law, energy devices would reradiate a portion of absorbed energy back to the Sun, resulting in inevitable power losses and consequent limitations on efficiency.[1] Most thermal emitters obey this law — that the emission and absorption remain identical — due to Lorentz reciprocity constraints.[2] However, advances in nanophotonics have enabled violation of Kirchhoff's law, allowing independent control over emissivity and absorptivity.[3–5] Nonreciprocal thermal emitters minimize radiation losses, enhancing energy conversion efficiency and enabling novel applications such as thermophotovoltaic devices and solar cells.[6,7]

Key strategies for achieving thermal nonreciprocity include the use of magneto-optical (MO) materials, time-varying systems, and nonlinear materials.[8–17] Zhu and Fan demonstrated that absorptivity and emissivity can be decoupled via the coupled-mode theory.[18] Experimental studies have further confirmed violations of Kirchhoff's law, resulting in a generalized formulation.[19–22] In photovoltaics and advanced thermal management, control of broadband and wide-angle radiation is crucial. Consequently, achieving broadband, wide-angle nonreciprocity remains a significant challenge in the field of NTR. Studies indicate that gradient epsilon-near-zero magnetized metamaterials enable continuous asymmetric Berreman mode excitation,[23] and broadband electromagnetic nonreciprocity has been experimentally verified.[24,25]

Another promising approach involves three-dimensional gapless topological materials, particularly magnetic Weyl semimetals (WSMs), which exhibit unique topological electronic states and break time-reversal symmetry.[26–30] Integrating dielectric gratings with WSMs has demonstrated broadband and wide-angle nonreciprocal radiation.[31,32] Shi *et al.* proposed WSM/dielectric multilayer thin-film structures that excite Brewster modes, achieving ultra-broadband and asymmetric angular emissivity.[33] Liu *et al.* further enhanced broadband nonreciprocal radiation by incorporating prisms into WSM gratings.[34] Additional techniques, such as MO lattice resonance, three-layer cavity enhancement and high-contrast gratings, and the introduction of new materials such as graphene, have extended the angular range of NTR.[35–38] Despite these advances, most broadband wide-angle nonreciprocity studies have focused on TM polarization. Wide-angle nonreciprocity with TM polarization shows a significant decline at angles greater than 60°, limiting its application

†Corresponding author. E-mail: sunxq@jlu.edu.cn

© 2026 Chinese Physical Society and IOP Publishing Ltd. All rights, including for text and data mining, AI training, and similar technologies, are reserved.

in solar energy collection. Compared with TM polarization, TE polarization excites no surface plasmon polaritons at the metal interface, thereby avoiding associated absorption losses and enabling wide-angle, broadband emission.[39] When integrated with high-index-contrast gratings, this configuration maintains large fabrication tolerances while significantly reducing thermal losses caused by metal absorption. Such a design shows great potential for realizing omnidirectional resonant absorption.[33,40,41] It is desirable to extend exploration to TE polarization to enhance the strength of NTR.

In this work, a TE-polarized wide-angle nonreciprocal emitter with optimized azimuthal angles is presented. Asymmetric wide-angle nonreciprocity at an incident wavelength of 16 μm is achieved. The proposed design exhibits high TE-polarized emission and low absorption over the azimuthal range from 20° to 80°. These findings contribute to the spectral, angular, and polarization control of thermal radiation, with potential applications in passive radiative cooling and adaptive infrared camouflage.

2. Device design

A schematic diagram of our proposed TE-polarized wide-angle nonreciprocal emitter is shown in Fig. 1. Owing to its high transparency and low propagation loss in the mid-infrared region, Ge has garnered significant attention in the field of photonic devices. Its well-characterized optical properties further contribute to reducing uncertainties in optical simulations.[42,43] Consequently, the structure proposed in this work consists of a periodic rectangular Ge grating, WSM, and a Ag reflective layer. The thicknesses of the grating and WSM are h_1 and h_2, respectively. The width and period of the gratings are w and d, respectively. The Ag reflective layer has a thickness of 200 nm to suppress all transmission. The angle between the incident plane and the x–z plane is φ, defined as the azimuthal angle. The considered TE-polarized light makes an angle of θ with the normal, denoted as the angle of incidence. In this work, the refractive index of Ge is 4.0. The permittivity of Ag is taken from Ref. [8]. In addition, an ideal magnetic WSM is considered with two Weyl nodes that have opposite chirality. The direction of momentum separation $2b$ is along the y-axis. Hence, the permittivity tensor of the WSM is denoted as[11,26,28]

$$\varepsilon = \begin{bmatrix} \varepsilon_{\mathrm{d}} & 0 & \mathrm{i}\varepsilon_{\mathrm{a}} \\ 0 & \varepsilon_{\mathrm{d}} & 0 \\ -\mathrm{i}\varepsilon_{\mathrm{a}} & 0 & \varepsilon_{\mathrm{d}} \end{bmatrix}. \tag{1}$$

The diagonal components ε_{d} and non-diagonal components ε_{a} of the permittivity tensor are[26]

$$\varepsilon_{\mathrm{a}} = \frac{be^2}{2\pi^2\hbar\omega\varepsilon_0}, \tag{2}$$

$$\varepsilon_{\mathrm{d}} = \varepsilon_{\mathrm{b}} + \mathrm{i}\frac{\sigma}{\omega}, \tag{3}$$

where ε_{b} and b represent the background conductivity and the axial vector of the WSM, respectively. The axial vector b is comparable to the external magnetic field of MO material, breaking the symmetry of the scattering matrix. σ represents the bulk conductivity, which is obtained from the random phase approximation to a two-band model with spin degeneracy. The bulk conductivity σ is calculated as[11]

$$\begin{aligned}\sigma = {} & \frac{r_{\mathrm{s}}g}{6}\Omega G\left(\frac{\Omega}{2}\right) + \mathrm{i}\frac{r_{\mathrm{s}}g}{6\pi}\left\{\frac{4}{\Omega}\left[1+\frac{\pi^2}{3}\left(\frac{k_{\mathrm{B}}T}{E_{\mathrm{F}}(T)}\right)^2\right]\right. \\ & \left. + 8\Omega\int_0^{\xi_{\mathrm{c}}}\frac{G(\xi)-G\left(\frac{\Omega}{2}\right)}{\Omega^2-4\xi^2}\xi\,\mathrm{d}\xi\right\},\end{aligned} \tag{4}$$

where $r_{\mathrm{s}} = e^2/4\pi\varepsilon_0\hbar v_{\mathrm{F}}$, $\Omega = \hbar\left(\omega + \mathrm{i}\tau^{-1}\right)/E_{\mathrm{F}}(T)$, and $\xi_{\mathrm{c}} = E_{\mathrm{c}}/E_{\mathrm{F}}(T)$ are the effective fine structure constant, the complex frequency normalized by the chemical potential, and the normalized cutoff energy, respectively. v_{F}, g, k_{B}, and τ^{-1} are the Fermi velocity, the number of Weyl points, the Boltzmann constant, and the scattering rate, respectively. Weyl nodes separated in momentum space are plotted in Fig. 1.

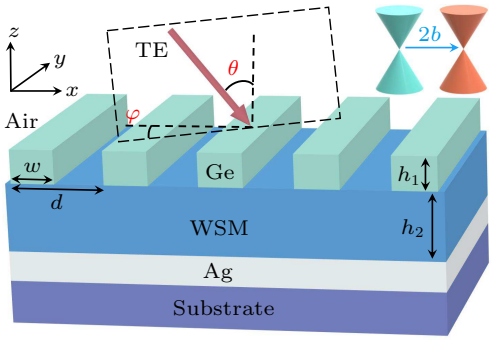


Fig. 1. Schematic diagram of the TE-polarized wide-angle nonreciprocal emitter. The cyan and orange electronic energy band structures indicate the momentum separation of paired Weyl nodes separated by $2b$ in the k_y direction.

The chemical potential $E_{\mathrm{F}}(T)$ of the WSM is sensitive to temperature, which is represented by[26]

$$E_{\mathrm{F}}(T) = \frac{2^{\frac{1}{3}}\left[9E_{\mathrm{F}}(0)^3 + \sqrt{81E_{\mathrm{F}}(0)^6 + 12\pi^6 k_{\mathrm{B}}^6 T^6}\right]^{\frac{2}{3}} - 2\pi^2 3^{\frac{1}{3}} k_{\mathrm{B}}^2 T^2}{6^{\frac{2}{3}}\left[9E_{\mathrm{F}}(0)^3 + \sqrt{81E_{\mathrm{F}}(0)^6 + 12\pi^6 k_{\mathrm{B}}^6 T^6}\right]^{\frac{1}{3}}}, \tag{5}$$

where $E_F(0) = 0.163$ eV. The parameters adopted in this study are taken from Refs. [11] and [26]: $b = 2 \times 10^9$ m^{-1}, $\varepsilon_b = 6.2$, $v_F = 0.83 \times 10^5$ m· s^{-1}, $g = 2$, $E_F = 0.15$ eV, $\tau = 1000$ fs, $T = 300$ K and $\xi = 3$. The selected parameters are similar to the published results for $Co_3Sn_2S_2$.[44] Here, the TE-polarized absorptivity $\alpha_s(\varphi, \theta, \lambda)$, emissivity $\varepsilon_s(\varphi, \theta, \lambda)$ and nonreciprocity $\eta(\varphi, \theta, \lambda)$ can be determined by the following equations:[20,27]

$$\alpha_s(\varphi_i, \theta_i, \lambda) = 1 - R_{ss}(\varphi_i, \theta_i, \lambda) - R_{sp}(\varphi_i, \theta_i, \lambda), \quad (6)$$

$$\varepsilon_s(\varphi_i, \theta_i, \lambda) = 1 - R_{ss}(\varphi_r, \theta_r, \lambda) - R_{ps}(\varphi_r, \theta_r, \lambda), \quad (7)$$

$$\eta(\varphi, \theta, \lambda) = \varepsilon_s(\varphi_i, \theta_i, \lambda) - \alpha_s(\varphi_i, \theta_i, \lambda). \quad (8)$$

$R_{s/p}(\varphi_i, \theta_i, \lambda)$ and $R_{s/p}(\varphi_r, \theta_r, \lambda)$ denote the reflectivity at symmetric incident angles, which can be obtained by rigorous coupled-wave analysis (RCWA).[45] Here, s and p denote TE and TM polarization, respectively, $\theta_i = \theta_r$ and $\varphi_r = \varphi_i + \pi$. Here, the parameter η is a dimensionless quantity, theoretically bounded between -1 and 1. Physically, $\eta = 0$ corresponds to the fulfillment of Kirchhoff's law, indicating that the structure operates in a reciprocal state. A nonzero value of η indicates that reciprocity in the emission–absorption process is broken, meaning the emissive capability at that specific incident direction or wavelength does not equal the absorptive capability under identical illumination conditions. Specifically, $\eta > 0$ indicates that emissivity exceeds absorptivity in that direction whereas $\eta < 0$ implies that absorptivity is greater than emissivity. Based on the value of η, tailored thermal emitters can be designed, and the structure can be applied to various thermal photonic applications, including radiative cooling. Following parameter optimization by RCWA, the geometrical parameters are $h_1 = 0.9$ μm, $h_2 = 0.5$ μm, $d = 5.5$ μm and $w/d = 0.6$.

3. Results and discussion

The absorption and emission spectra at an azimuthal angle of 42° were calculated and are shown in Fig. 2. It can be seen that the emitter exhibits nonreciprocal absorption and emission over a wide angular range around the incident light at a wavelength of 16 μm. This asymmetric emission and absorption become more pronounced at larger incident angles. Therefore, an incident angle of 76° is considered here. In this case, the emissivity, absorptivity and nonreciprocity are plotted in Fig. 3. At $\varphi = 42°$ and $\theta = 76°$, the device shows high radiation and low absorption within the wide wavelength range from 15.5 to 16.5 μm. In Fig. 3(a), the nonreciprocity exceeds 0.6 in a 0.3 μm wide wavelength range. NTR over a wide angular range can be achieved at an incident wavelength of 16 μm, as shown in Fig. 3(b). Further analysis shows that the absorption and radiation spectra almost separate and the nonreciprocity surpasses 0.6 within the 38.4° angular range.

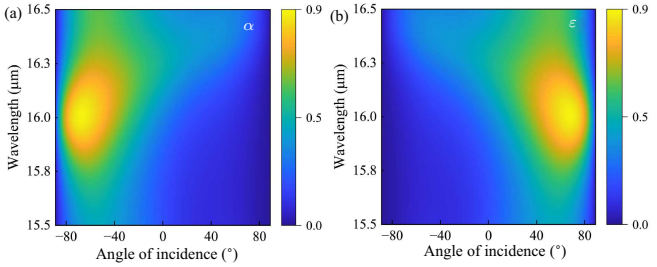


Fig. 2. Asymmetric wide-angle (a) absorption and (b) emission spectra plotted at $\varphi = 42°$.

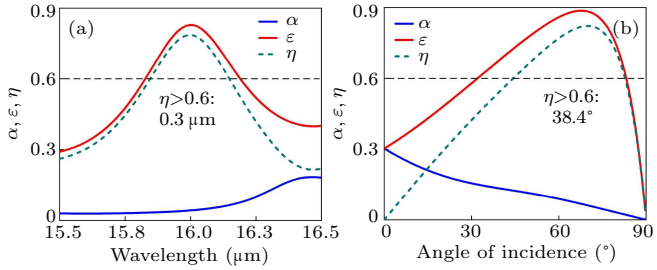


Fig. 3. (a) Absorptivity α, emissivity ε and nonreciprocity η versus wavelength with $\varphi = 42°$ and $\theta = 76°$. (b) Absorptivity α, emissivity ε and nonreciprocity η as a function of the incident angle with $\varphi = 42°$ and $\lambda = 16$ μm.

Thereby, the proposed emitter can violate the conventional Kirchhoff's law of thermal radiation in a wide angular range. TE-polarized wide-angle nonreciprocity reaches up to 82%. This wide-angle behavior arises because the nonreciprocity, induced by the intrinsic topological properties of WSMs, is not confined to small angles of incidence. Moreover, the high-refractive-index Ge grating supports strongly confined guided-mode resonances (GMRs), where the high degree of modal field overlap enhances the coupling strength and leads to improved angular tolerance. The Ag layer breaks the structural symmetry via the direction-dependent reflection phase, and cooperates with the nonreciprocal scattering from the grating–WSM layer, collectively resulting in a pronounced nonreciprocal response across a wide angular range.[25,32] This strong nonreciprocity stems from the anomalous Hall effect associated with Weyl nodes, which is converted into off-diagonal complex components of the dielectric tensor through the transverse conductivity σ_{xy}. The presence of nonzero σ_{xy} gives rise to nonvanishing off-diagonal elements in the dielectric tensor, thereby generating a pronounced nonreciprocal response.[26,28]

To better explain the mechanism behind the broadband nonreciprocity, the electric field distribution is analyzed at different incident angles, as shown in Fig. 4. Under the conditions of $\lambda = 16$ μm and $\varphi = 42°$, the distribution of the electric field component $|E_y|^2$ is simulated at incident angles of 20°, 40°, 60°, and 80° and their corresponding opposite (negative) angles. Most electric field power is distributed at the interface between the Ge layer and the air, as well as dissipating into the air, which leads to low absorption by the proposed structure. Obviously, there are huge differences in the electric field distributions between opposite angles, which is an important

reason for the nonreciprocity. As the angle of incidence gradually increases, this difference gradually increases too. The nonreciprocity also undergoes the same change, which is consistent with the results shown in Fig. 3(b). Figure 5 shows the reflectivity, emissivity, and transmissivity spectra of the proposed structure, where the emissivity equals the absorption rate in the opposite direction to incidence. A distinct reflection dip is observed at the resonance wavelength of $\lambda = 16$ μm, accompanied by a peak in emissivity and near-zero transmittance. These features indicate that incident light at the resonance couples into lower-order waveguide modes through the periodic grating and dissipates within the Ge layer, exhibiting distinct critical coupling behavior that directly demonstrates the existence of GMR.

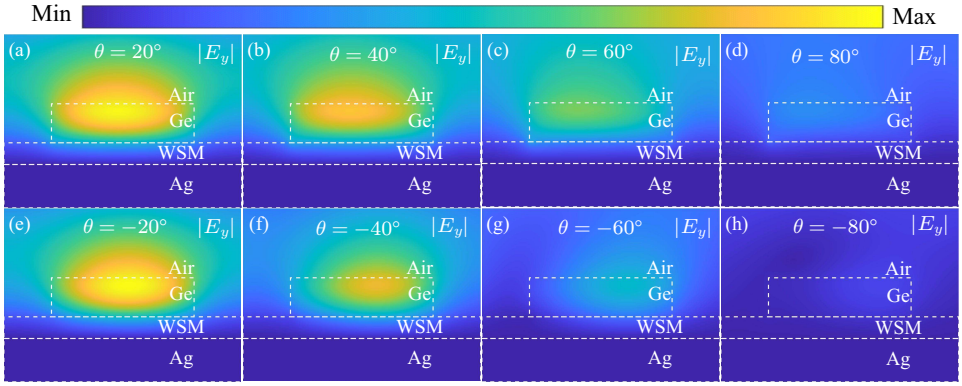


Fig. 4. The electric field distribution $|E_y|^2$ diagram of the wide-angle nonreciprocal emitter with incident angles of (a) 20°, (b) 40°, (c) 60°, (d) 80°, (e) −20°, (f) −40°, (g) −60° and (h) −80° for $\lambda = 16$ μm and $\varphi = 42°$.

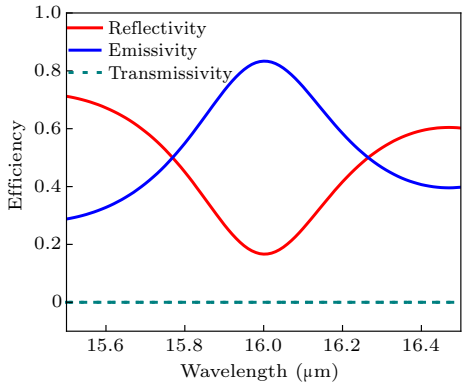


Fig. 5. The reflectivity, emissivity and transmissivity spectra when $\varphi = 42°$ and $\theta = 76°$ for TE polarization.

As is well known, the strong nonreciprocity of TE polarization is attributed to the contribution of the azimuthal angle.[46] Therefore, we now analyze in detail the effect of azimuthal angle on TE-polarized wide-angle performance. The incident angle θ ranges from 0° to 89°, and the azimuthal angle φ ranges from 0° to 360°. The dependence of the emissivity, absorptivity, and nonreciprocity on the azimuthal angle is plotted in Fig. 6 for $\lambda = 16$ μm. As expected, TE polarization has no nonreciprocity observed in the plane with $\varphi = 0$. The emitter exhibits wide-angle high emission and low absorption for TE polarization over the azimuth angle range from 20° to 80°, which indicates the excellent robustness of the proposed emitter. The nonreciprocity is calculated in Fig. 6(c). Within the range of azimuthal angle from 30° to 60°, TE-polarized wide-angle nonreciprocity over 70% can be achieved. Compared with previous wide-angle nonreciprocal thermal radiators,[31–36] this proposed design effectively implements wide-angle nonreciprocity operation in the case of TE polarization. With respect to practical scenarios, the impact of geometrical size fluctuations on the emissivity is considered in Fig. 7. The absorption decreases slightly over the wide angular range when the thickness h_1 of the Ge grating increases from 0.85 μm to 0.95 μm. The absorption shows good stability over the wide angular range when the thickness h_2 of the WSM increases from 0.45 μm to 0.55 μm. In addition, as the period d varies from 4.1 μm to 6.7 μm, the absorption shows a similar variation pattern to that seen with variation of thickness h_2. Wide-angle nonreciprocal emitters with excellent fabrication tolerances will be attractive in thermal management and energy applications.

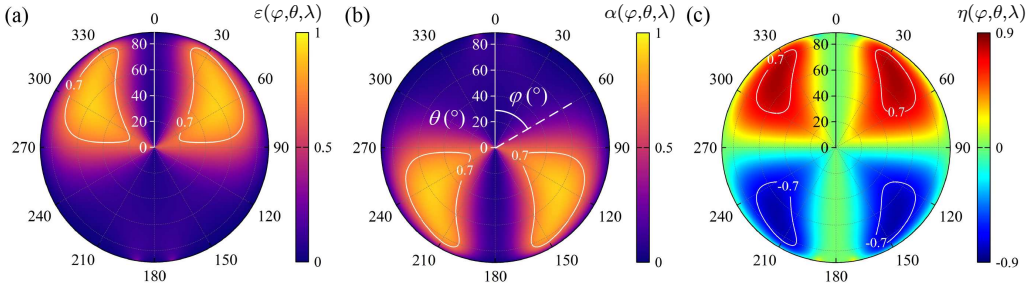


Fig. 6. (a)–(c) The dependence of emissivity $\varepsilon(\varphi,\theta,\lambda)$, absorptivity $\alpha(\varphi,\theta,\lambda)$ and nonreciprocity $\eta(\varphi,\theta,\lambda)$ on the azimuthal angle at $\lambda = 16$ μm, respectively. The incident angle θ ranges from 0° to 89° and the azimuthal angle φ ranges from 0° to 360°.

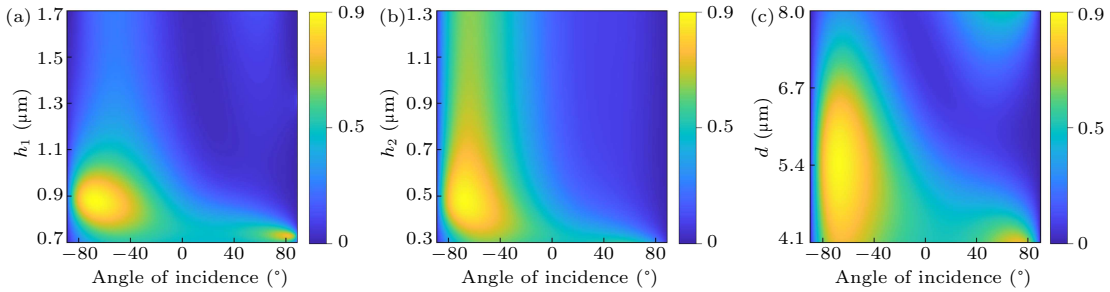


Fig. 7. The wide-angle asymmetric absorption carries fluctuations in the geometrical parameters (a) h_1, (b) h_2 and (c) d for $\lambda = 16$ μm and $\varphi = 42°$.

Table 1. Comparison of recent nonreciprocal devices.

Reference	Structure	Polarization	η	θ (°)
[27]	Si grating + WSM + Ag	TM	> 0.94	20–80
[32]	Ge–WS grating + Ag	TM	> 0.9	36–64.5
[33]	Multilayered WSM + dielectric	TM TE	≈ 1 ≈ 0	16–88
[34]	WSM grating + Ag	TM	> 0.9	40–80
[35]	SiO_2–InAs grating + Ag cavity	TM	> 0.8	0–89
[36]	Dielectric + WSM + dielectric	TM	> 0.98	0–90
[37]	SiO_2 grating + dielectric + WSM	TM TE	> 0.92 > 0.94	38 20–70
[38]	Ag grating + WSM + graphene + dielectric	TM	> 0.8	39–80
This work	Ge grating + WSM + Ag	TE	> 0.8	44.4–82.8

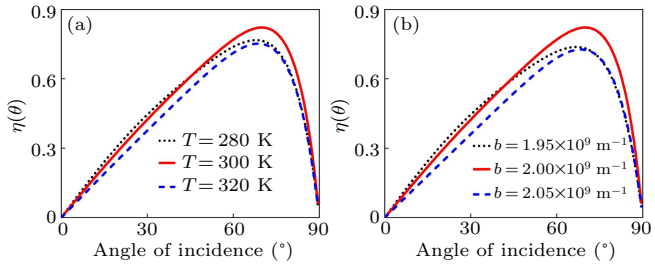


Fig. 8. Dependence of wide-angle nonreciprocity on (a) temperature and (b) axial vectors of WSMs at $\lambda = 16$ μm, $\theta = 76°$ and $\varphi = 42°$.

The nonreciprocal thermal emission structures reported recently[31–38] are summarized in Table 1, including key parameters such as the supported polarization, nonreciprocity, and angular range. It can be seen that most high-performance nonreciprocal emitters are in works involving TM polarization and exhibit extremely low nonreciprocity in TE polarization.[33] Although nonreciprocity in TE polarization was achieved in Ref. [37], the structure is relatively complex. In contrast, the structure proposed in this work has a nonreciprocal emission rate greater than 0.8 in TE polarization with a wide angular range of 44.4° to 82.8°, which is comparable to reported TM-polarized devices.

In previous reports, the permittivity of WSMs was sensitive to temperature.[12,26] The axial vector can be altered by external magnetic excitation,[47] and the axial vector directly affects the non-diagonal component. Therefore, the effect of temperature and axial vector on nonreciprocity is considered in Fig. 8. The effect of temperature change has an unremarkable impact on TE-polarized wide-angle nonreciprocity. Similar to the scenario of temperature, wide-angle nonreciprocity shows favorable stability in the case of a slight increase in the axial vector, as shown in Fig. 8(b).

The following procedure was adopted for the fabrication of the proposed structure. In this plan, a Si wafer is selected as the substrate and a Ag layer is deposited via electron beam evaporation or magnetron sputtering, as illustrated in Fig. 9(a).[48–50] Subsequently, a WSM layer is grown on the Ag reflective layer using molecular beam epitaxy or radiofrequency magnetron sputtering, corresponding to Fig. 9(b).[51,52] Figure 9(c) shows the deposition of a sufficiently thick Ge layer onto the WSM via thermal evaporation.[53] The photoresist is then spin-coated onto the Ge surface, resulting in the multilayer structure presented in Fig. 9(d). Through photolithography and development, a mask with the desired duty cycle is formed, as shown in Fig. 9(e). Figure 9(f) illustrates the reactive ion etching process to form a Ge layer with the desired thickness.[54] Finally, the mask is removed, yielding the target grating structure depicted in Fig. 9(g).

The surface morphology of the grating can be examined using atomic force microscopy to verify the geometric size and configuration of the periodic structure. Focused ion beam cross-sectioning combined with scanning electron microscopy can be employed to inspect the cross-sectional profile, allowing precise measurement of layer thickness, grating verticality, duty cycle, and interfacial adhesion quality.[55] Repeated measurements can be performed and averaged to ensure consistency between the fabricated device parameters and simulated counterparts. The emissivity of the structure can be measured by Fourier-transform infrared spectroscopy, while the absorptivity can be characterized using a J. A. Woollam IR-VASE ellipsometer. The overall nonreciprocity can be determined through subsequent computational analysis.[25]

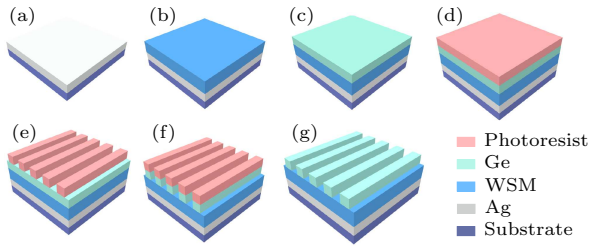


Fig. 9. Manufacturing process of a wide-angle nonreciprocal WSM emitter. Utilizing magnetron sputtering to deposit (a) Ag layers and (b) WSM layers. (c) The Ge layer on the WSM layer can be prepared using thermal evaporation. (d) Spin-coating of photoresist on the Ge layer, followed by then exposure and development to obtain (e). (f) Reactive ion etching to obtain the Ge grating structure and removal of the residual photoresist to obtain (g) a wide-angle nonreciprocal WSM emitter.

4. Conclusion

In conclusion, a TE-polarized wide-angle nonreciprocal thermal emitter with strong nonreciprocity across a broad range of azimuthal and incident angles is presented. The proposed emitter exhibits excellent fabrication tolerance and remains robust against variations in temperature and the axial vector of WSMs. Compared with previous approaches, the proposed design breaks the limitation of wide-angle nonreciprocity on TM polarization. It contributes to the technology of energy harvesting, showing potential for use in medical sensing, directional thermal camouflage, and thermal management.

Data availability statement

Data underlying the results presented in this paper are not publicly available at this time but may be obtained from the authors upon reasonable request.

Acknowledgement

This study was supported by the Science and Technology Research Project of Jilin Provincial Education Department (Grant No. JJKH20250106KJ).

References

[1] Li W, Buddhiraju S and Fan S 2020 *Light Sci. Appl.* **9** 68
[2] Kirchhoff G 1860 *Ann. Phys.* **185** 275
[3] Zhang Z and Zhu L 2022 *Phys. Rev. Appl.* **18** 027001
[4] Yang S, Liu M, Zhao C, Zhao C, Fan S and Qiu C W 2024 *Nat. Photonics* **18** 412
[5] Fang J, Wang M, Yue J, Sun Z, Sun X, Wu Y and Zhang D 2023 *Int. Commun. Heat Mass Transfer* **148** 107031
[6] Ghalekohneh S J and Zhao B 2022 *Phys. Rev. Appl.* **18** 034083
[7] Green M A 2012 *Nano Lett.* **12** 5985
[8] Zhao B, Shi Y, Wang J, Zhao Z, Zhao N and Fan S 2019 *Opt. Lett.* **44** 4203
[9] Li J, Wu Z, Zhang D, Sun Y, Liu W and Yu T 2024 *Opt. Lett.* **49** 1313
[10] Fang J, Zou J, Liu T, Wang Y, Sun X, Wu X, Wu Y and Zhang D 2024 *Int. J. Heat Mass Transfer* **223** 125229
[11] Asadchy V S, Guo C, Zhao B and Fan S 2020 *Adv. Opt. Mater.* **8** 2000100
[12] Fang J, Zou J, Liu T, Wang M, Sun X, Wu Y and Zhang D 2024 *Appl. Phys. Lett.* **124** 171702
[13] Qing Y M, Liu J, Yang Z, Wu L W, Gou Y, Wu J and Li B 2025 *Opt. Lett.* **50** 1552
[14] Ghanekar A, Wang J, Guo C, Fan S and Povinelli M L 2022 *ACS Photonics* **10** 170
[15] Ghanekar A, Wang J, Fan S and Povinelli M L 2022 *ACS Photonics* **9** 1157
[16] Cotrufo M, Cordaro A, Sounas D L, Polman A and Alù A 2023 *Nat. Photonics* **18** 81
[17] Wu X, Liu R, Yu H and Wu B 2021 *J. Quant. Spectrosc. Radiat. Transf.* **272** 107794
[18] Zhu L and Fan S 2014 *Phys. Rev. B* **90** 220301
[19] Guo C, Zhao B and Fan S 2022 *Phys. Rev. X* **12** 021023
[20] Zhang Z M, Wu X and Fu C 2020 *J. Quant. Spectrosc. Radiat. Transf.* **245** 106904
[21] Shayegan K J, Zhao B, Kim Y, Fan S and Atwater H A 2022 *Sci. Adv.* **8** eabm4308
[22] Shayegan K J, Biswas S, Zhao B, Fan S and Atwater H A 2023 *Nat. Photonics* **17** 891
[23] Liu M, Xia S, Wan W, Qin J, Li H, Zhao C, Bi L and Qiu C W 2023 *Nat. Mater.* **22** 1196
[24] Zhang Z and Zhu L 2023 *Phys. Rev. Appl.* **19** 014013
[25] Shayegan K J, Hwang J S, Zhao B, Raman A P and Atwater H A 2024 *Light Sci. Appl.* **13** 176
[26] Zhao B, Guo C, Garcia C A C, Narang P and Fan S 2020 *Nano Lett.* **20** 1923
[27] Wu J and Qing Y M 2024 *Int. Commun. Heat Mass Transfer* **151** 107254
[28] Guo C, Asadchy V S, Zhao B and Fan S 2023 *eLight* **3** 2
[29] Wu J, Wang Z, Zhai H, Shi Z, Wu X and Wu F 2021 *Opt. Mater. Express* **11** 4058
[30] Wu X, Yu H, Wu F and Wu B 2021 *AIP Adv.* **11** 075106
[31] Wu J, Sun Y, Wu B, Wang Z and Wu X 2022 *Case Stud. Therm. Eng.* **40** 102566
[32] Wu J and Qing Y M 2023 *Appl. Phys. Lett.* **122** 012203
[33] Shi K, Sun Y, Hu R and He S 2024 *Nanophotonics* **13** 737
[34] Liu Z, Li H, Xiao J, Luo F, Chen J, Cui R, Li Z, Shen J and Li C 2024 *Opt. Express* **32** 30642
[35] Wang J, Shi K and Xing X 2024 *Mater. Today Phys.* **46** 101515
[36] Wang Z, Xu S, Zheng G, Qian L and Pei S 2024 *Opt. Lett.* **49** 262
[37] Wu J and Qing Y M 2024 *Int. Commun. Heat Mass Transfer* **156** 107639
[38] Qing Y M and Wu J 2024 *Res. Phys.* **60** 107657
[39] Zakharian A R, Moloney J V and Mansuripur M 2007 *Opt. Express* **15** 183
[40] Chung I S 2015 *Opt. Express* **23** 16730
[41] Liu D, Yu H, Duan Y, Li Q and Xuan Y 2016 *Sci. Rep.* **6** 32515
[42] Marris-Morini D, Vakarin V, Ramirez J M, Liu Q, Ballabio A, Frigerio J, Montesinos M, Alonso-Ramos C, Le Roux X, Serna S, Benedikovic D, Chrastina D, Vivien L and Isella G 2018 *Nanophotonics* **7** 1781
[43] Torre A D, Sinobad M, Armand R, Luther-Davies B, Ma P, Madden S, Mitchell A, Moss D J, Hartmann J M, Reboud V, Fedeli J M, Monat C and Grillet C 2021 *APL Photon.* **6** 016102
[44] Wang Q, Xu Y, Lou R, Liu Z, Li M, Huang Y, Shen D, Weng H, Wang S and Lei H 2018 *Nat. Commun.* **9** 3681
[45] Li L 2003 *J. Opt. A: Pure Appl. Opt.* **5** 345
[46] Wu J, Wu B, Shi K, Wu X and Fu C 2023 *Int. J. Therm. Sci.* **187** 108172
[47] Li P G, Koo J, Ning W, Li J, Miao L, Min L, Zhu Y, Wang Y, Alem N, Liu C X, Mao Z and Yan B 2020 *Nat. Commun.* **11** 3476
[48] Barman P, Deka A, Mondal S, Chowdhury D and Bhattacharyya S 2020 *J. Phys. D: Appl. Phys.* **53** 325302
[49] Depla D 2022 *Coatings* **12** 1915
[50] McPeak K M, Jayanti S V, Kress S J P, Meyer S, Iotti S, Rossinelli A and Norris D J 2015 *ACS Photonics* **2** 326
[51] Li S, Gu G, Liu E, Cheng P, Feng B, Li Y, Chen L and Wu K 2020 *ACS Appl. Electron. Mater.* **2** 126
[52] Okamura Y, Minami S, Kato Y, Fujishiro Y, Kaneko Y, Ikeda J, Muramoto J, Kaneko R, Ueda K, Kocsis V, Kanazawa N, Taguchi Y, Koretsune T, Fujiwara K, Tsukazaki A, Arita R, Tokura Y and Takahashi Y 2020 *Nat. Commun.* **11** 4619
[53] Sorianello V, Colace L, Armani N, Rossi F, Ferrari C, Lazzarini L and Assanto G 2011 *Opt. Mater. Express* **1** 856
[54] Lindblom M, Reinspach J, von Hofsten O, Bertilson M, Hertz H M and Holmberg A 2009 *J. Vac. Sci. Technol. B* **27** L1
[55] Xie Q, Shchedrina N, Cavillon M, Poumelleca B and Lancry M 2024 *Nanoscale Adv.* **6** 489